International Journal of Engineering Research and Science & Technology

www.ijerst.org

ISSN : 2319-5991

Vol. 22 No. 3 (2026)

ijerst.editor@gmail.com

editor@ijerst.com

ISSN 2319-5991 www.ijerst.com

Peer Reviewed, Referred & Indexed Journal

Research Paper

Two-Dimensional Scramjet Engine Inlet Design and Computational Fluid Dynamics Analysis for Mach 6 Flight

AVASALI DINESHKUMAR[1], Mrs. V. SARITHA[2], Dr.B. SANDHYA RANI[3]
[1]PG Student, CAD/CAM, Ellenki College of Engineering and Technology.
[2]Asst. Prof., Department of Mechanical Engineering, Ellenki College of Engineering and Technology.
[3]Head of the Dept., Department of Mechanical Engineering, Ellenki College of Engineering and Technology.

Abstract - Because it uses the forward momentum of the vehicle to compress the incoming air rather than spinning compressor and turbine hardware, the supersonic combustion ramjet (scramjet) is one of the most promising air-breathing propulsion ideas for sustained flight beyond Mach 5. Performance at the inlet directly affects the efficiency of combustion downstream and net thrust in this configuration because it is responsible for capturing air from the free stream, increasing its pressure through a sequence of oblique shocks, and delivering a relatively uniform, high-pressure flow to the combustor while limiting total-pressure loss. In this work, we detail the planning and analysis of a two-dimensional scramjet intake with two ramps, optimized for Mach 6 operation at 30 km altitude. We used standard oblique-shock relations and a shock-on-lip criterion to size the inlet geometry, which consists of two compression ramps, a cowl, and a constant-area isolator duct. We then built the model as a solid in CATIA V5. After that, we imported it into ANSYS Fluent to do compressible-flow analysis with a density-based solver and the SST k-ϋ turbulence model. Before applying the same meshing strategy to the designed inlet for an inviscid run, a two-dimensional viscous run, and a three-dimensional viscous run capturing sidewall effects, a mesh-dependency study was performed on a previously validated two-ramp inlet geometry to fix an appropriate cell size. We compare the three-dimensional analysis, the inviscid and viscous CFD findings, and the one-dimensional design calculations. As compared to the inviscid case, the results demonstrate that the captured air is gradually compressed through the ramp shock system while the flow remains supersonic all the way to the isolator exit. In the viscous solution, there is measurable shock displacement and localized flow separation near the ramp-cowl shoulder. Additionally, the three-dimensional analysis reveals that there is sidewall-driven non-uniformity that fades within about 8 mm of the side surfaces. The design point pressure recovery and flow uniformity are both within acceptable ranges, suggesting that the geometry is a good starting point for a Mach 6 scramjet inlet. However, there are some areas that need further refinement, specifically viscous, off-design, and sidewall effects.

Terms for Index - Computerized fluid dynamics, scramjet intake, hypersonic flight, oblique shock, SST k-ϋ, pressure recovery, compressible flow, and ANSYS Fluent are all part of the picture.

I. INTRODUCTION

Conventional turbojet and turbofan engines are unable to meet the propulsion demands of flights above Mach 5 due to the aerodynamic heating and mechanical loads experienced at hypersonic speed [1, 2]. This has kept people interested in air-breathing concepts that can keep combustion going in those kinds of environments. One of the better ones is the scramjet, which stands for supersonic combustion ramjet and uses the vehicle's forward speed to compress the incoming air rather than any rotating machinery. It's simpler and lighter than a turbine-based alternative, and it can keep combustion going as long as the engine flow stays supersonic. By design, a scramjet typically consists of an intake, an isolator, a combustion chamber, and an exhaust nozzle. While maintaining supersonic flow, the inlet compresses the collected air using a series of oblique shocks; the isolator then reduces pressure fluctuations before the combustor; fuel, usually hydrogen, is injected and burned quickly in the combustor under supersonic conditions; and the resulting hot, high-energy gas is expanded through the nozzle to produce thrust. A poorly functioning inlet can cause engine unstart, boundary-layer separation, or excessive pressure loss [3, 4]. The inlet determines the temperature, pressure, and uniformity of the air that enters the engine, so its aerodynamic quality directly affects combustion stability, pressure recovery, and overall propelling efficiency.

Before building a physical prototype, it is possible to evaluate the inlet aerodynamics, including pressure fields, shock structure, temperature rise, and velocity change, using computational tools like CATIA V5 for solid geometry and ANSYS Fluent for compressible-flow simulation [5]. A two-dimensional, two-ramp scramjet inlet designed for Mach 6 flight at 30 km altitude was evaluated computationally in this article. We used oblique-shock theory to size the inlet geometry, which was then solid-modeled in CATIA V5. We then used ANSYS Fluent, a density-based solver, and the SST k-ö turbulence model to evaluate the inlet design. We started by doing a mesh-dependency and validation exercise on a previously tested reference geometry, and then we ran inviscid, two-dimensional viscous, and three-dimensional viscous analyses to make sure the inlet was aerodynamically suitable for future hypersonic propulsion development.

II. REVIEW OF LITERATURE

Due to its potential for high specific impulse and high flight speeds, air-breathing hypersonic propulsion has been the subject of persistent study in the defense and space launch sectors [6]. To circumvent the significant shock losses and combustor temperatures caused by subsonic diffusion at flight speeds exceeding approximately Mach 5, a scramjet maintains the flow supersonic throughout, in contrast to a traditional ramjet that slows the flow to subsonic before combustion [3]. The main function of a scramjet is to maintain the combustor inlet at a specific static-temperature and static-pressure ratio throughout the entire flight envelope. This is done with the best possible compression efficiency and total-pressure recovery [4]. The inlet controls the engine's starting behavior and total-pressure recovery, making it a crucial part of the vehicle's design [3, 4], [7]. From NASA's Hyper-X program, which aimed for Mach 5 flight, to the HyShot experiment, which proved practical scramjet propulsion for the first time, to the HIFiRE flight research series, which confirmed sustained scramjet operation in multiple flight tests, and finally, to the X-51A Waverider, which proved the technology's viability, scramjet inlets have been steadily improved through ground and flight research programs. Managing the structural and thermal demands placed on intake materials by the enormous dynamic pressures and temperatures of hypersonic flight, as well as ensuring stable operation under these circumstances, are persistent issues [4].

There are a number of documented approaches to designing two-dimensional scramjet inlets. All ramp shocks converge at the cowl lip with identical shock intensity in Roberts's three-ramp, Mach-4 mixed-compression intake, which maximizes total-pressure ratio, adiabatic compression ratio, kinetic-energy efficiency, and entropy increase using the stream-thrust approach [12]. Using an evolutionary optimization strategy, Brown [2] determined that a blunted, viscous configuration outperformed the corresponding inviscid, sharp-edged case for an external compression inlet with three ramps and a Mach-10 rating, when subjected to a shock-on-lip criterion, an internal contraction limit, and combustor-flow constraints. Torrez [13] expanded this method and tested it with a five-ramp, external-compression intake operating at Mach 7-9 at various incidence angles and flying speeds. Predicting scramjet inlet performance using CFD has been frequently used. In his study, Idris [1] used ANSYS Fluent's density-based, second-order upwind solver with Roe flux-difference splitting to analyze a Mach-5 inlet with two ramps and the SST k-ö turbulence model and a low-Reynolds-number correction. He then compared the results to experimental data to validate the wall pressures and numerical Schlieren images, which is the same validation approach used in this study. Su [15] used an SST k-ö model with compressibility correction and a MUSCL scheme to study the transient restart behavior of a three-dimensional inlet along a flight trajectory, while Nguyen [14] used an in-house solver with a flux-splitting scheme and k-ö closure to examine sidewall compression and relaminarization in a three-dimensional inlet. There have been reports of complementary experimental programs at several locations. Using Z-type color Schlieren imaging, ramp pressure tappings and transducers, pressure-sensitive paint, and infrared thermography, Idris [1] tested a two-ramp Mach-5 inlet model in the blowdown supersonic tunnel at the University of Manchester. Using a pitot rake and an extensive pressure-tapping array, Hohn [16] investigated a single-ramp Mach-7 inlet with variable internal contraction, while Häberle [17] used shadowgraph visualisation and a conical-plug flow meter to simulate combustor back-pressure to characterize a two-ramp Mach-7 inlet flow field. Taken as a whole, these works define the technique used for the design of the inlet under consideration here, as well as the CFD/experimental validation strategy that was used.

III. STUDY DESIGN

A. Governing Relations and Design Point

Due to their importance in determining free-stream static pressure, static temperature, and speed of sound through the standard atmosphere, the design Mach number and cruising altitude were set first. The standard θ-β-M relation was used to calculate the downstream Mach number, static-pressure ratio, static-temperature ratio, and total-pressure ratio across each shock, and each compression ramp was viewed as an oblique shock of angle β that turned the flow through a deflection angle Θ. The corresponding compressible-flow oblique-shock relations were relied upon for these calculations [18]. These relationships are applied in a certain order for a multi-ramp intake, where each shock's input is the Mach number and flow angle.

The design was limited by four constraints: a shock-on-lip criterion that requires all ramp shocks to intersect at the cowl lip under certain conditions in order to maximize captured mass flow; an equal-pressure-ratio condition across the ramps to minimize the overall entropy rise for a given total compression; a Kantrowitz-limit / internal-contraction-ratio check to ensure that the inlet can self-start without requiring variable geometry; and combustor-entry limits on isolator-exit static temperature and Mach number to maintain a stable supersonic combustion downstream. The steps in the design process included settling the design Mach number, ramp count, and an initial ramp-angle estimate; repeatedly solving the θ-β-M relation for each ramp to get the shock angles and downstream Mach numbers; simultaneously solving for ramp angles and lengths using the shock-on-lip and equal-pressure-ratio conditions; checking the resultant geometry against the Kantrowitz starting limit; computing the isolator-exit Mach number, static pressure, and static temperature to make sure they were within acceptable combustor limits; and lastly fixing the ramp angles, ramp lengths, cowl height, and isolator length that were utilized in the CAD model. We may see the resultant geometric characteristics in Table I.

Table I: Finished Inlet Geometric Parameters

Parameter	Symbol	Value
First ramp angle	θ_1	8°
Second ramp angle	θ_2	12°
First ramp length	x_1	60 mm
Second ramp length	x_2	70 mm
Isolator length	x_3	90 mm
Throat (cowl) height	h_3	18 mm
Inlet capture height	h_1	35 mm
Inlet span (width)	–	50 mm
Overall inlet length	–	220 mm

In order to isolate the effects of viscous and boundary layers, which are not included in the one-dimensional treatment, and to compare the subsequent CFD results to, we first used the oblique-shock relations in this section to get a preliminary one-dimensional estimate of Mach number, static pressure, static temperature, and total pressure at each compression station.

B. Solid modeling in CATIA V5

Utilizing the Sketcher and Part Design workbenches, the intake geometry—consisting of the forebody compression ramps, cowl, and isolator duct—was constructed in CATIA V5. After setting up reference planes at the origin, the two-dimensional ramp-and-cowl profile was drawn using the ramp angles and lengths from Table I. Then, to produce the three-dimensional solid, the profile was extruded to the necessary inlet span using a Pad operation. After the cowl lip, a constant-area isolator duct section was added. To smooth out any unnatural sharp edges, dress-up fillets were used as required. Lastly, the ramps, cowl, and isolator were merged into one piece. Before being exported in STEP format for input into ANSYS, the finished solid was double-checked against the Table I dimensions using CATIA's measurement and geometry-verification tools. It was exhibited in an isometric perspective alongside the typical front/top/side orthographic arrangement.

C. Boundary conditions, CFD model, and mesh

The computational fluid dynamics (CFD) studies were executed in ANSYS Fluent with the help of a density-based, compressible, steady-state solver that incorporated second-order upwind spatial discretization. The SST k-ϋ turbulence model was chosen for its proven effectiveness in flows characterized by hypersonic inlets' boundary-layer interactions and strong adverse pressure gradients [1]. In Table II, we can see a summary of the Mach 6 design case's general solver and free-stream flow parameters.

Parameters for the Solver and Free-Stream Flow (Table II)

Parameter	Value
Gas constant (R)	287 J/kg·K
Specific heat at constant pressure (Cp)	1004.5 J/kg·K
Free-stream density (ρ_0)	0.018 kg/m³
Speed of sound (a_0)	301.8 m/s
Free-stream velocity (V∞)	1810.8 m/s (Mach 6)
Dynamic viscosity (μ)	1.46×10^{-5} kg/m·s
Turbulence model	SST k–ω
Solver type	Density-based
Flow type	Compressible, steady-state

The numerical method was first evaluated using published Mach-5 wind tunnel and computational fluid dynamics (CFD) data on a two-ramp inlet shape before the planned inlet was analyzed [1]. Mach 5 flight, 62.5 K static temperature, and 1220 Pa static pressure were the boundary conditions for the validation scenario. With cell counts of 41,576, 83,012, and 166,024 respectively, all three structured meshes were constructed in a mesh-dependency research. Each mesh maintained wall y+ below unity, and the maximum cell sizes were 1 mm, 0.5 mm, and 0.25 mm. In Table III, we can see how the three meshes' output conditions compare.

TABLE III. Examination of Mesh Dependency—Geometry for Validation

Mesh #	Max. Cell Size (mm)	Cell Count	Outlet Static Pressure (Pa)	Outlet Mach No.	Outlet Mass Flow (kg/s)
1	1.0	41,576	23,012	1.98	1.432
2	0.5	83,012	23,372	1.96	1.420
3	0.25	166,024	23,577	1.94	1.425

The meshing strategy and numerical model were determined to be appropriate for the analysis of the designed inlet because the relative difference between Mesh #2 and Mesh #3 was less than 1% for outlet static pressure, Mach number, and mass flow rate. Mesh #2 was considered to provide a mesh-independent solution, and its numerical Schlieren image and outlet velocity profile were compared with the corresponding experimental data. Both showed a consistent ramp-shock structure and similar shock/separation locations within the isolator. As a means of evaluating convergence in all runs, residuals were driven down to 10^{-4} and the isolator-outlet mass-weighted average Mach number, static pressure, total pressure, and mass flow rate were tracked until they stabilized. Additionally, a net mass-flow imbalance throughout the control volume was considered until it approached zero. Next, the designed inlet was subjected to three analyses using the validated meshing strategy: a two-dimensional inviscid run that matched the inviscid assumption used for sizing, a two-dimensional viscous run that included boundary-layer effects, and a three-dimensional viscous run that captured interactions with the sidewalls. For both inviscid and viscous two-dimensional runs, the free-stream boundary conditions were Mach 6 flight at 30 km altitude, with a static pressure of 1161.18 Pa and a static temperature of 231.61 K, holding the wall temperature constant. In these cases, the mesh had a maximum cell size of 0.5 mm, yielding about 112,160 cells, which is in agreement with the mesh-dependency results mentioned earlier. The three-dimensional model made use of first-order upwind spatial discretization and a hexcore mesh consisting of about 17.08 million cells, with a maximum cell width of 0.5 mm.

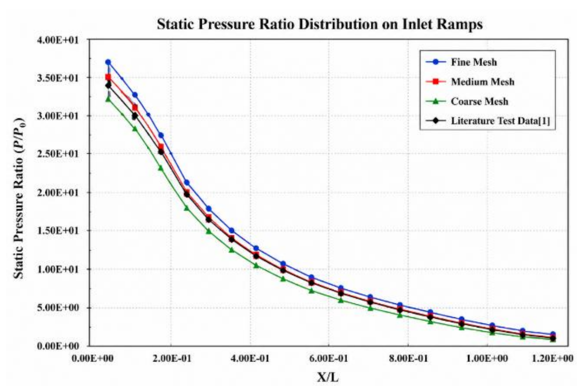

Figure 1. Analysis of the Distribution of Static Pressure Ratios on Inlet Ramps

IV. THE OUTCOME

This section gives the one-dimensional design estimate, the inviscid and viscous two-dimensional CFD results, and the three-dimensional CFD results for the intended intake, combined with a comparison across these scenarios.

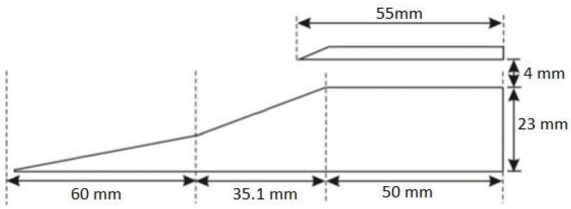

Figure 2. An Inlet for 2D Scramjet Design

A. Single-Dimensional Schematic Projection

At the end of each compression stage and at the isolator exit, for the design Mach-6 condition—which is used as a baseline for comparing the CFD results in the following subsections—Table IV lists the one-dimensional Mach number, static pressure, static temperature, and total pressure.

Table IV: The Designed Inlet's Projected One-Dimensional Performance

Parameter	Value	Parameter	Value
M_1	4.73	P_{S1}	3.980 kPa
M_2	3.64	P_{S2}	13.610 kPa
M_3 (isolator exit)	2.30	P_{S3}	68.280 kPa
T_1	346.90 K	Pt_1	15.267 bar
T_2	519.50 K	Pt_2	12.714 bar
T_3	923.20 K	Pt_3	8.525 bar

B. Analyse van inviscide CFD

The inviscid, two-dimensional CFD run reproduced the shock-on-lip condition targeted in the design, with the numerical Schlieren image confirming that both ramp shocks intersect at the cowl lip as intended. Table V compares the inviscid CFD results against the one-dimensional estimate of Table IV using mass-weighted averages; Mach numbers after each compression stage differ from the one-dimensional prediction by roughly 0.2–4.6%, static pressures by roughly 0.1–2.4%, and static temperatures by roughly 0.3–4.1%, while total pressure shows a larger deviation of 15–17%, attributable to the multi-dimensional shock and expansion effects captured by CFD but not represented in the one-dimensional treatment. These deviations were judged acceptable and consistent with the expected differences between a one-dimensional estimate and a resolved compressible-flow solution.

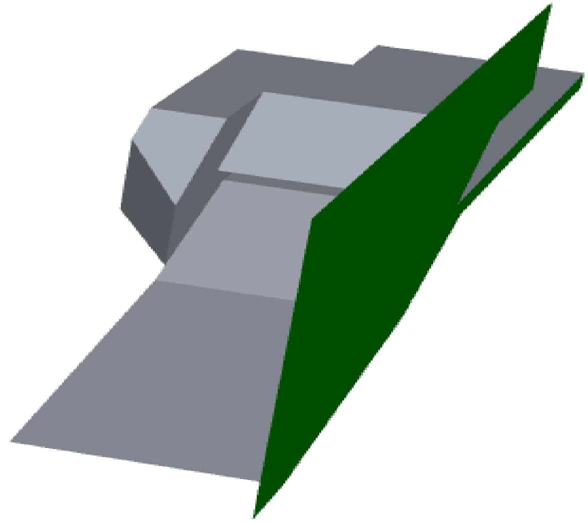

Figure 3. Graph of Symmetry and Plane

TABLE V. Comparison of Inviscid CFD Results with 1D Estimate

Parameter	CFD Value	Diff. (%)	Parameter	CFD Value	Diff. (%)
M_1	4.74	0.21	P_{S1}	3.920 kPa	1.53
M_2	3.65	0.27	P_{S2}	13.626 kPa	0.12
M_3	2.41	4.56	P_{S3}	66.690 kPa	2.38
T_1	343.00 K	1.14	Pt_1	18.420 bar	17.12
T_2	518.00 K	0.29	Pt_2	15.060 bar	15.58
T_3	887.00 K	4.08	Pt_3	10.300 bar	17.23

C. Viscous CFD Analysis

A numerical Schlieren pattern differed significantly from the inviscid case when viscous effects were introduced to the identical mesh and boundary conditions. This difference was shown as observable displacement of the ramp shocks and localised flow separation at the shoulder at the end of the second ramp. Table VI shows that when comparing the viscous and inviscid solutions, there are significant changes in Mach-number (2.6-11.6%), static-pressure (3-11%), and total-pressure (6-16%). This is because the inviscid solution does not account for the additional total-pressure loss caused by boundary-layer growth and shock/boundary-layer interaction. In spite of these discrepancies, the intake starts up without a hitch and operates in viscous circumstances rather near to the design purpose, according to the performance metrics and contour fields taken combined.

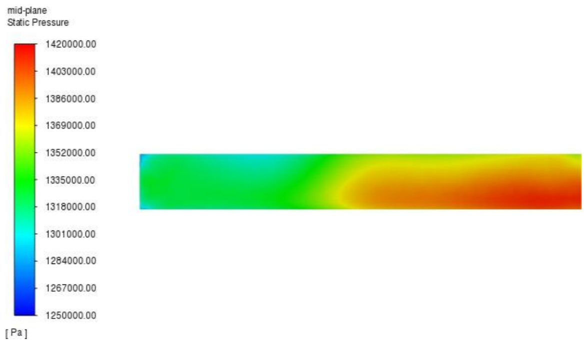

Figure 4. 3-Dimensional Outlet Static Pressure Curve

Comparing Viscous CFD Methods (Table VI) Findings using Inviscid CFD Models

Parameter	Viscous Value	Diff. (%)	Parameter	Viscous Value	Diff. (%)
M_1	4.62	2.60	P_{s1}	4.39 kPa	−10.71
M_2	3.54	3.11	P_{s2}	14.05 kPa	−3.02
M_3	2.16	11.57	P_{s3}	74.12 kPa	−10.02
T_1	355 K	−3.38	P_{t1}	17.3 bar	6.47
T_2	540 K	−4.07	P_{t2}	13.2 bar	14.09
T_3	980 K	−9.49	P_{t3}	8.9 bar	15.73

D. Sidewall Effects and Three-Dimensional CFD Analysis

In order to identify any sidewall-driven three-dimensional flow features that were not captured by the two-dimensional model, the whole intake geometry was subjected to a three-dimensional viscous computational fluid dynamics (CFD) study. Table VII shows that there were relative differences of 3.9%, 4.5%, and 6.5% at the three compression stations when comparing the two-dimensional viscous case to the geometry's symmetry plane, which means that the two-dimensional analysis captures the core compression behaviour reasonably well.

Comparison of 3D Symmetry-Plane with 2D Outcomes (Table VII)

Parameter	Relative Difference (%)
M_1	3.90
M_2	4.52
M_3	6.48

When looking at Mach curves on planes that were getting closer and closer to the sidewall, it was evident that there was flow disturbance very next to the wall. The disturbance became less as one got farther away from the wall, and at about 8 mm from the wall, it looked almost like the symmetry-plane structure. The two-dimensional analysis accurately depicts the bulk compression process, but the local compression ratio near the sidewalls is significantly lower than the core flow, indicating that sidewall interaction significantly impacts the flow quality that reaches the combustor. Despite this, the Mach-number distribution at the isolator outlet is nearly uniform.

V. THEME DEBATE

The findings as a whole lend credence to the shape as a feasible baseline for a Mach 6 scramjet intake, but there are a few things that need more explanation. It is worth noting that the design-stage oblique-shock calculations accurately represent the inviscid compression process, as indicated by the close agreement (generally under 5%) between the one-dimensional estimate and the inviscid CFD result for Mach number, static pressure, and static temperature. On the other hand, the much larger discrepancy in total pressure (15-17%) is a result of the limitations of a one-dimensional, single-streamline treatment in representing the multi-dimensional shock structure resolved by CFD. This discrepancy should be seen as a property of the comparison method rather than a sign of a design deficiency. The second reason an inviscid design calculation isn't enough for a scramjet inlet is because the viscous solution causes noticeable changes such as ramp-shock displacement, shoulder-region separation, and a consistent decrease in total pressure at every station. This is because the sizing stage ignored viscous, boundary-layer, and shock-interaction effects, which significantly alter the shock pattern and the pressure recovery actually delivered to the isolator. Any credible performance claim, then, must be based on the viscous solution, not the inviscid design point. Thirdly, the three-dimensional analysis reveals that the two-dimensional model, although sufficient for predicting core compression behaviour to a degree of approximately 6.5%, fails to account for the non-uniformity caused by the sidewalls, which is evident in the outlet compression ratio.

This suggests that a specific mechanism that a two-dimensional design study would miss is the interaction between the boundary layer and the flow around the corners, especially for a narrow-span inlet where the sidewall-affected region occupies a larger percentage of the overall width. Lastly, a dedicated experimental or independently documented CFD comparison for the Mach 6 designed inlet itself would further strengthen this conclusion, since the mesh-dependency and validation exercise was conducted on an independently tested reference geometry instead of the designed inlet itself. The confidence gained from that validation transfers to the present results only to the extent that the two geometries and flow regimes are aerodynamically similar.

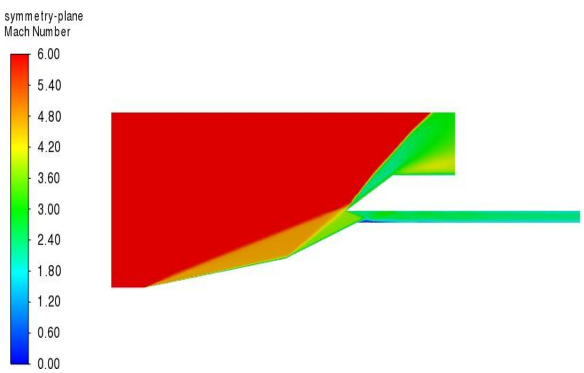

Figure 5. Mach Contour-Dynamic Finite Element-Symmetry Plane

VI. CONCLUSION

Using standard oblique-shock relations under shock-on-lip and equal-pressure-ratio constraints, a two-ramp, two-dimensional scramjet inlet was designed for Mach 6 flight at 30 km altitude. The design was then implemented as a solid in CATIA V5, and the evaluation was carried out in ANSYS Fluent using a density-based solver and the SST k-ὒ turbulence model. The developed inlet was subjected to inviscid, two-dimensional viscous, and three-dimensional viscous assessments after a suitable meshing strategy was determined by a mesh-dependency and validation research on a previously tested reference inlet. The one-dimensional design Mach number, pressure, and temperature estimates were within 5% in the inviscid CFD solution, which replicated the intended shock-on-lip compression pattern, and in the viscous solution, there was measurable shock displacement, shoulder-region separation, and reduced total-pressure recovery compared to the inviscid case. The two-dimensional model correctly depicts core compression behaviour, according to the three-dimensional study, but it underestimates the sidewall-driven flow non-uniformity, which decreases the local compression ratio along the side surfaces at the isolator exit. All things considered, the results show that the designed inlet maintains supersonic flow through the isolator exit, compresses the captured flow efficiently, and has pressure recovery and flow uniformity within acceptable ranges at the design point. This geometry can be used as a foundation for future hypersonic inlet development. The particular next steps to further support this inlet's aerodynamics include expanding the design and computational fluid dynamics (CFD) analysis to off-design flying situations, conducting dedicated experimental validation of the Mach 6 geometry, and refining the shape to reduce sidewall losses.

REFERENCES

[1] A. C. Idris, "Characterization of High-Speed Inlets Using Global Measurement Techniques," Ph.D. dissertation, University of Manchester, 2014.

[2] M. Brown, N. Mudford, A. Neely, and T. Ray, "Robust design optimization of two-dimensional scramjet inlets," in 14th AIAA/AHI Space Planes and Hypersonic Systems and Technologies Conf., Nov. 2006, doi: 10.2514/6.2006-8140.

[3] S. Torrez, J. Driscoll, D. Dalle, and M. Fotia, "Preliminary design methodology for hypersonic engine flowpaths," in 16th AIAA/DLR/DGLR Int. Space Planes and Hypersonic Systems and Technologies Conf., Oct. 2009, doi: 10.2514/6.2009-7289.

[4] M. K. Smart, "Optimization of two-dimensional scramjet inlets," J. Aircraft, vol. 36, no. 2, pp. 430–433, Mar. 1999, doi: 10.2514/2.2448.

[5] W. H. Heiser and D. T. Pratt, Hypersonic Airbreathing Propulsion. Washington, DC: American Institute of Aeronautics and Astronautics, 1994.

[6] E. T. Curran and S. N. B. Murthy, Eds., Scramjet Propulsion, vol. 189. Reston, VA: AIAA, 2001.

[7] S. O'Byrne, M. Doolan, S. R. Olsen, and A. F. P. Houwing, "Measurement and imaging of supersonic combustion in a model scramjet engine," Shock Waves, vol. 9, no. 4, pp. 221–226, Aug. 1999, doi: 10.1007/s001930050159.

[8] NASA, "NASA Armstrong Fact Sheet: Hyper-X Program," NASA, 2014.

[9] M. K. Smart, N. E. Hass, and A. Paull, "Flight data analysis of the HyShot 2 scramjet flight experiment," AIAA Journal, vol. 44, no. 10, pp. 2366–2375, Oct. 2006, doi: 10.2514/1.20661.

[10] T. J. Juliano, D. Adamczak, and R. L. Kimmel, "HIFiRE-5 flight test results," J. Spacecraft and Rockets, vol. 52, no. 3, pp. 650–663, May 2015, doi: 10.2514/1.A33142.

[11] J. Hank, J. Murphy, and R. Mutzman, "The X-51A scramjet engine flight demonstration program," in 15th AIAA Int. Space Planes and Hypersonic Systems and Technologies Conf., Apr. 2008, doi: 10.2514/6.2008-2540.

[12] K. Roberts and D. Wilson, "Analysis and design of a hypersonic scramjet engine with a transition Mach number of 4.00," in 47th AIAA Aerospace Sciences Meeting, Jan. 2009, doi: 10.2514/6.2009-1255.

[13] S. Torrez, J. Driscoll, D. Dalle, and M. Fotia, "Design and analysis of a five-ramp external-compression scramjet inlet across a Mach 7–9 flight envelope," in 16th AIAA/DLR/DGLR Int. Space Planes and Hypersonic Systems and Technologies Conf., Oct. 2009, doi: 10.2514/6.2009-7289.

[14] T. Nguyen, M. Behr, B. Reinartz, O. Hohn, and A. Gülhan, "Effects of sidewall compression and relaminarization in a scramjet inlet," J. Propulsion and Power, vol. 29, no. 3, pp. 628–638, May 2013, doi: 10.2514/1.B34740.

[15] W.-Y. Su, Z. Hu, P.-P. Tang, and Y. Chen, "Transient analysis for hypersonic inlet accelerative restarting process," J. Spacecraft and Rockets, vol. 54, no. 2, pp. 376–385, Mar. 2017, doi: 10.2514/1.A33601.

[16] O. M. Hohn and A. Gülhan, "Experimental characterization of three-dimensional scramjet inlet with variable internal contraction," J. Propulsion and Power, vol. 38, no. 1, pp. 71–83, Jan. 2022, doi: 10.2514/1.B38315.

[17] J. Häberle and A. Gülhan, "Investigation of two-dimensional scramjet inlet flowfield at Mach 7," J. Propulsion and Power, vol. 24, no. 3, pp. 446–459, May 2008, doi: 10.2514/1.33545.

[18] J. D. Anderson Jr., Modern Compressible Flow: With Historical Perspective, 3rd ed. New York, NY: McGraw-Hill, 2003.